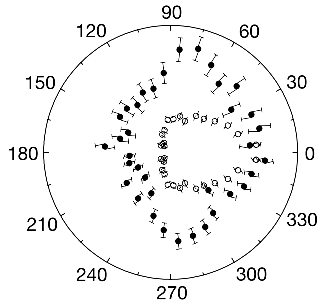

Figure 4 Triply differential single ionization cross-sections for the perpendicular plane for 2 MeV per a.m.u. C^{6+} + He collisions. Open symbols, $E_e = 4$ eV, $q = 0.7$ a.u.; solid symbols, $E_e = 1$ eV, $q = 1.5$ a.u.

relative to $\mathbf{q}'$. If this rotation, which does not affect the direction of the electron momentum, is 90°, the electron ends up in the perpendicular plane ($\mathbf{p}_o$, $\mathbf{q}'$) which started off as the scattering plane after the initial projectile–electron interaction. Because the electron does not take part in the second step, its polar angular distribution remains unchanged leading to a peak at the same angle as in the scattering plane.

This mechanism has an important impact on basic features characteristic to ionization which were previously thought to be understood. What appears to be a recoil peak in the scattering plane emerges as a 'recoil ring' in the measured three-dimensional electron emission pattern, which is nearly isotropic with respect to rotation about the projectile beam axis. This behaviour, not reproduced by theory, can also be explained qualitatively by the mechanism suggested above: if the projectile–target nucleus interaction leads to a rotation of $\mathbf{q}$ about the projectile beam axis by 180° then the ionized electron is emitted in the direction of $-\mathbf{q}$ (that is, it looks like a 'recoil peak electron'), although it was not backscattered by the target nucleus. This could be an important contributor to the recoil peak, which so far has not been discussed in the literature. Such contributions would also explain small but systematic underestimations of the height of the recoil peak by theory both for electron and ion impact[1,13,17]. Of course, the projectile–target nucleus interaction can lead to any rotation of $\mathbf{q}$ between 0° and 180° thus giving rise to the observed ring shape.

This process represents a potentially important few-body effect involving all collision products. In principle, it is contained in the final state wavefunction in our calculation. Furthermore, we note that, for the sake of a graphic explanation, our description of this mechanism represents a simplification. The CDW–HF model treats this process more realistically in that here the projectile–electron and projectile–target nucleus interactions do not occur sequentially, but instead simultaneously. However, the final state wavefunction is only asymptotically exact when at least one of the collision products is at a large distance from the other two particles. Its accuracy is not known when all particles are close together. But this process is expected to be important exactly when all collision products are still close together and may therefore be significantly underestimated by the calculation.

Very recently, in a promising theoretical development, the CDW-approach has been generalized to include non-zero magnetic sub-states in the final state wavefunction[14]. Such sub-states would be expected to contribute to the cross-sections out of the scattering plane and therefore offer an alternative or complementary explanation to the one proposed above. However, numeric calculations on fully differential cross-sections with this method are not yet available.

Existing theoretical approaches should be tested relative to their capability of reproducing measured three-dimensional electron emission patterns. Such tests may reveal that qualitatively new theoretical concepts need to be developed in order to achieve a better understanding of ionization processes even at large projectile energies. The data presented here represent experimental progress for such efforts. Obtaining a satisfactory description of atomic few-body processes, in turn, is an important step towards a better understanding of the general few-body problem. □

Received 26 July; accepted 16 December 2002; doi:10.1038/nature01415.

1. Ehrhardt, H., Jung, K., Knoth, G. & Schlemmer, P. Differential cross sections of direct single electron impact ionization. *Z. Phys. D* **1,** 3–32 (1986).
2. Stefani, G., Avaldi, L. & Camilloni, R. On the relevance of the final ionic state to the (e,2e), TDCS. *J. Phys. B* **23,** L227–L231 (1990).
3. Lahmam-Bennani, A. Recent developments and new trends in (e,2e) and (e,3e) studies. *J. Phys. B* **24,** 2401–2442 (1991).
4. Murray, A. J., Woolf, M. B. J. & Read, F. H. Results from symmetric and non-symmetric energy sharing (e,2e) experiments in the perpendicular plane. *J. Phys. B* **25,** 3021–3036 (1992).
5. Röder, J., Ehrhardt, H., Bray, I., Fursa, D. V. & McCarthy, I. E. Absolute triple differential cross-section for electron-impact ionization of helium at 40 eV. *J. Phys. B* **29,** 2103–2114 (1996).
6. Schulz, M. *et al.* Triply differential single ionization cross-sections in coplanar and non-coplanar geometry for fast heavy ion-atom collisions. *J. Phys. B* **34,** L305–L311 (2001).
7. Ehrhardt, H., Schulz, M., Tekaat, T. & Willmann, K. Ionization of helium: angular correlation of the scattered and ejected electrons. *Phys. Rev. Lett.* **22,** 82–92 (1969).
8. Bray, I. & Stelbovics, A. T. Explicit demonstration of the convergence of the close-coupling method for a Coulomb three-body problem. *Phys. Rev. Lett.* **69,** 53–56 (1992).
9. Rescigno, T. N., Baertschy, M., Isaacs, W. A. & McCurdy, C. W. Collisional breakup in a quantum system of three charged particles. *Science* **286,** 2474–2479 (1999).
10. Belkic, Dz. A quantum theory of ionisation in fast collisions between ions and atomic systems. *J. Phys. B* **11,** 3529–3552 (1978).
11. Crothers, D. S. F. & McCann, J. F. Ionisation of atoms by ion impact. *J. Phys. B* **16,** 3229–3242 (1983).
12. Jones, S. & Madison, D. H. Evidence of initial-state two-center effects for (e,2e) reactions. *Phys. Rev. Lett.* **81,** 2886–2889 (1998).
13. Madison, D., Schulz, M., Jones, S., Foster, M., Moshammer, R. & Ullrich, J. Comparison of theoretical and absolute experimental fully differential cross sections for ion-atom impact ionization. *J. Phys. B* **15,** 3297–3314 (2002).
14. Crothers, D. S. F. *et al.* Magnetically quantized continuum distorted waves. *Phys. Rev. Lett.* **88,** 053201–053204 (2002).
15. Ullrich, J. *et al.* Recoil-ion, momentum spectroscopy. *J. Phys. B* **30,** 2917–2974 (1997).
16. Whelan, C. T., Allan, R. J., Walters, H. R. J. & Zhang, X. in *(e,2e) and Related Processes* (eds Whelan, C. T., Walters, H. R. J., Lahmam-Bennani, A. & Ehrhardt, H.) Vol. 414 of *Series C: Mathematical and Physical Sciences* 1–32 (Kluwer, Dordrecht, 1993).
17. Marchalant, P., Whelan, C. T. & Walters, H. R. J. Second-order effects in (e,2e) excitation-ionization of helium to He^{+} (n = 2). *J. Phys. B* **31,** 1141–1178 (1998).

Acknowledgements We thank W. Schmitt, R. Mann, R. Dörner, T. Weber, Kh. Khayyat, A. Cassimi, L. Adoui, J. P. Grandin and staff members of the CIRIL for their help performing the experiment at the GANIL; thanks to R. E. Olson and J. Fiol for discussions. The support of the Deutsche Forschungsgemeinschaft within the Leibniz-program, by GSI, the European Union, the NSF and by CIRIL (GANIL at Caen) is acknowledged.

Competing interests statement The authors declare that they have no competing financial interests.

Correspondence and requests for materials to M.S. (e-mail: schulz@umr.edu).

Ordering and manipulation of the magnetic moments in large-scale superconducting π-loop arrays

Hans Hilgenkamp*, Ariando*, Henk-Jan H. Smilde*, Dave H. A. Blank*, Guus Rijnders*, Horst Rogalla*, John R. Kirtley† & Chang C. Tsuei†

* *Faculty of Science and Technology and MESA^{+} Research Institute, University of Twente, P.O. Box 217, 7500 AE Enschede, The Netherlands*
† *IBM T. J. Watson Research Center, Yorktown Heights, New York 10598, USA*

The phase of the macroscopic electron-pair wavefunction in a superconductor can vary only by multiples of 2π when going around a closed contour. This results in quantization of magnetic flux, one of the most striking demonstrations of quantum phase coherence in superconductors[1–3]. By using superconductors with unconventional pairing symmetry[4–7], or by incorporating π-Josephson junctions[8], a phase shift of π can be introduced in

such loops[7,9,10]. Under appropriate conditions, this phase shift results in doubly degenerate time-reversed ground states, which are characterized by the spontaneous generation of half quanta of magnetic flux, with magnitude 1/2 Φ_0($\Phi_0 = h/2e = 2.07 \times 10^{-15}$ Wb) (ref. 7). Until now, it has only been possible to generate individual half flux quanta. Here we report the realization of large-scale coupled π-loop arrays based on $YBa_2Cu_3O_7$-Au-Nb Josephson contacts[11,12]. Scanning SQUID (superconducting quantum interference device) microscopy has been used to study the ordering of half flux quanta in these structures. The possibility of manipulating the polarities of individual half flux quanta is also demonstrated. These π-loop arrays are of interest as model systems for studying magnetic phenomena—including frustration effects—in Ising antiferromagnets[13–18]. Furthermore, studies of coupled π-loops can be useful for designing quantum computers based on flux-qubits[19–23] with viable quantum error correction capabilities[24,25].

The half-flux-quantum effect in single π-loops has been used in various phase-sensitive pairing symmetry tests to provide an unambiguous signature for *d*-wave order parameter pairing symmetry in high-transition-temperature (high-T_c) copper oxide superconductors[7,9], and as a potentially practical application of *d*-wave superconductivity[10]. These experiments were mainly conducted by using grain boundaries in high-T_c superconductors, induced by the epitaxial deposition on tri- or tetracrystalline substrates[7,10] or by using Josephson junctions between a conventional superconductor and $YBa_2Cu_3O_7$ (ref. 9).

However, the techniques used thus far for the fabrication of π-loops do not lend themselves to the construction of coupled π-loop arrays. To this end, we have developed thin-film ramp-type $YBa_2Cu_3O_7$-Au-Nb Josephson contacts, with high critical current density; the fabrication procedure of these contacts has been described in detail in refs 11 and 12. First, bilayers of 150-nm [001]-oriented $YBa_2Cu_3O_7$ and 100-nm $SrTiO_3$ are epitaxially grown by pulsed-laser deposition on [001]-oriented $SrTiO_3$ single-crystal substrates. In these bilayers, the basic layout of the structures that generate half flux quanta, which will be described below, is defined by photolithography and Ar-ion milling. This process results in interfaces with a slope of 15–20° with respect to the substrate, which provides access to the *a*–*b* planes of the $YBa_2Cu_3O_7$ and allows the exploitation of *d*-wave phase effects. Special care is taken to align all interfaces accurately along one of the $YBa_2Cu_3O_7$ ⟨100⟩ axes. After etching the ramp and cleaning the sample, a 7-nm $YBa_2Cu_3O_7$ interlayer is deposited (the function and properties of which are described in ref. 12), followed by the *in situ* pulsed-laser deposition of a 6-nm Au barrier layer. A 160-nm Nb counter electrode is then formed by d.c. sputtering and structured by lift-off. Subsequently, the redundant, uncovered Au is removed by ion milling.

Each chip contained several reference junctions. At temperature $T = 4.2$ K, these showed a typical critical current per micrometre junction width of $I_c/w \approx 0.1\ \mathrm{mA\,\mu m^{-1}}$. From this, a value for the Josephson penetration depth $\lambda_j \approx 1\ \mu$m ($T = 4.2$ K) is deduced, which is the characteristic length scale over which Josephson vortices (fluxons) extend. The sample magnetic fields were imaged with a high-resolution scanning SQUID microscope[26–29]. The SQUID microscope images shown here were made at a temperature of 4.2 K, with the sample cooled and imaged in a magnetic induction $<0.5\ \mu$T. The images of Figs 1 and 2 were made with an octagonal pick-up loop 4 μm in diameter; the image of Fig. 3 was made with a square pick-up loop 8 μm on a side.

The first configuration for which we investigated the generation and coupling of half-integer flux quanta is the zigzag array[11], shown schematically in Fig. 1a inset. In this structure, the *d*-wave order parameter of the $YBa_2Cu_3O_7$ induces a difference of π in the Josephson phase shift $\Delta\phi$ across the $YBa_2Cu_3O_7$-Au-Nb barrier for neighbouring facets. For facet lengths *a* in the wide limit, that is, $a \gg \lambda_j$, the lowest-energy ground state of the system is expected to be characterized by the spontaneous generation of a half-integer flux quantum at each corner. This half-fluxon provides a further π-phase change between neighbouring facets, either adding or subtracting to the *d*-wave induced π-phase shift, depending on the half-flux-quantum polarity. In both cases, this leads to a lowering of the Josephson coupling energy across the barrier, as this energy is proportional to $(1 - \cos\Delta\phi)$.

In the scanning SQUID microscopy image presented in Fig. 1a, a spontaneously induced magnetic flux is clearly seen at every corner of the zigzag structure. For this sample $a = 40\ \mu$m, which implies that the facets are well within the wide limit. The observed corner fluxons are arranged in an antiferromagnetic fashion. This antiferromagnetic ordering was found to be very robust, occurring for many cool-downs and for different samples with comparable geometries. Deviations from an antiferromagnetic arrangement were only observed when a magnetic field was applied during cool-down, or when an Abrikosov vortex was found trapped in (or near) the junction interface. The total flux per Josephson vortex in the faceted array of Fig. 1a was estimated to be $\Phi = 0.42 \pm 0.12\Phi_0$ by fitting the observed integrated flux through the SQUID pick-up

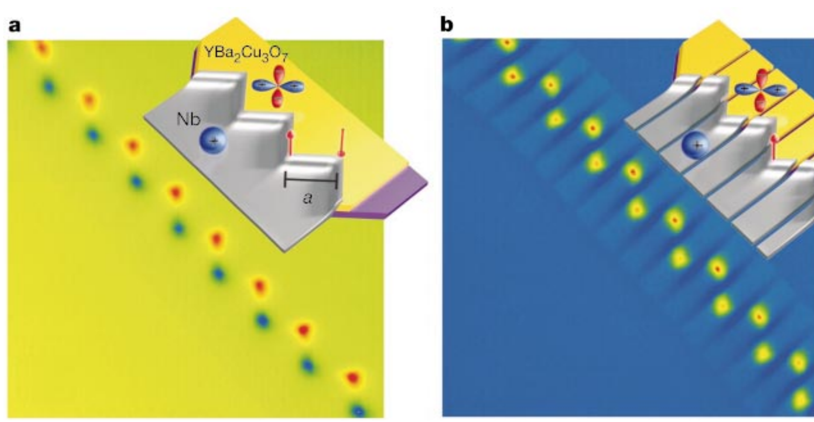

Figure 1 Generation of half flux quanta in connected and unconnected $YBa_2Cu_3O_7$-Au-Nb zigzag structures. Shown are scanning SQUID micrographs of **a**, 16 antiferromagnetically ordered half-integer flux quanta at the corners of a connected zigzag structure, and **b**, 16 ferromagnetically ordered half flux quanta at the corners of an unconnected zigzag tructure ($T = 4.2$ K). The geometries of the structures are shown schematically in the insets. The purple and yellow layers represent the $YBa_2Cu_3O_7$-$SrTiO_3$ bilayer; the Nb layer is indicated in grey. The *s*-wave and *d*-wave order parameter symmetries of the Nb and the $YBa_2Cu_3O_7$ are represented by the round and four-leaved-clover-shaped icons, respectively. The facet length *a* is 40 μm in these measurements. In **a**, the yellow–red dots represent flux with opposite polarity to the blue dots, with the zero background flux indicated in green. In **b**, all corner fluxes have the same polarity and are presented by the yellow–red dots, the zero background flux now being indicated in blue.

loop to a model of an array of magnetic monopole sources with alternating signs, localized at the meeting points of the facets[7]. The Josephson vortices were quite uniform, as evidenced by a standard deviation of the observed peak heights of about 0.12 times the average peak height.

In the zigzag configuration, all the half-fluxons are generated in a singly connected superconducting structure; the question therefore arises as to whether the antiferromagnetic ordering is due to a magnetic interaction between the fractional fluxons, or to an interaction via the superconducting connection between the corners. To investigate this, we have also fabricated arrays of corner junctions, in a similar configuration as the zigzag arrays but with 2.5-μm-wide slits etched halfway between the corners. In this situation there is no superconducting connection between the separate flux-generating corner junctions. For a distance between the corners equal to the facet length in the connected array, $a = 40\,\mu$m, a ferromagnetic arrangement of the fractional flux quanta was observed (Fig. 1b). The magnetic interaction between the half flux quanta at these distances is expected to be very weak, and alignment along minute spurious background fields in the scanning SQUID microscope is anticipated to be the dominating mechanism for their parallel arrangement. When the distance was decreased to about 20 μm, with a slit width of 1.5 μm, a tendency towards an antiferromagnetic coupling was observed. This was explored further in coupled two-dimensional arrays, which will be described below.

By comparing the behaviour of the connected and the unconnected arrays, we conclude that the antiferromagnetic ordering in the connected zigzag array with $a = 40\,\mu$m (Fig. 1a) arises through the phase of the wavefunction in this singly connected superconducting structure. We propose that the basic mechanism for this is the following. During cool-down, the zigzag array undergoes a transition from the small to the wide facet limit, as the Josephson penetration depth is inversely proportional to the square root of the junctions' critical current density. During this transition the flux is generated, converging ultimately to 1/2 Φ_0 in the limit $\lambda_j \ll a$. For the intermediate regime, $\lambda_j \approx a$, the flux is smaller—the facet length being too small to accommodate a complete half-fluxon. In that case, to obtain overall the lowest energy state, the phase change associated with the flux generated at one corner is compensated with an equal, but opposite, phase-change at the neighbouring corner, yielding an antiferromagnetic arrangement of the fractional fluxes. When cooled down further, this antiferromagnetic ordering freezes in, and the fractional fluxes grow to complete half-integer flux quanta.

For unconnected corner junctions at sufficiently close distances, the half flux quanta are becoming antiferromagnetically arranged owing to magnetic interaction. To further explore this, we have realized two-dimensional triangular arrays. This geometry is of particular interest, as with a preferential antiferromagnetic coupling between the half-integer flux quanta, it provides a model example of a strongly frustrated system, characterized by a highly degenerate ground state[13]. Until now, such systems have been studied with, for example, arrays of all-low-T_c superconducting rings biased at an external magnetic flux of 1/2 Φ_0 per ring[16,17], and with low-T_c Josephson junction arrays (see, for example, ref. 18 and references therein). Fluctuations in the dimensions of those rings, resulting in variations in the flux bias and a lifting of the degeneracy, have been found to be a major complication in these investigations[16]. The spontaneously generated flux in the $YBa_2Cu_3O_7$-Au-Nb structures provides an advantage in this respect, as the two flux states in these elements are intrinsically degenerate.

Figure 2 depicts a scanning SQUID micrograph of the arrangement of the fractional flux quanta in a section of such a triangular array. For this sample, the distance between the half-fluxons is 12 μm. In total, about 25,000 half flux quanta were achieved on a single chip, of size 5 mm × 10 mm.

We verified the predominantly antiferromagnetic nearest-neighbour interaction by determining the bond-order parameter σ, following the method described in refs 16 and 30. In this method, $\sigma = 1 - (n_{AF}/2x_+x_-)$, with n_{AF} the fraction of antiferromagnetic bonds, and $x_+(x_-)$ the concentrations of half-integer flux quanta pointing upwards (downwards), respectively. For $\sigma < 0$, an additional fraction of antiferromagnetic bonds exists, as compared with the completely random arrangement, which yields $\sigma = 0$. For

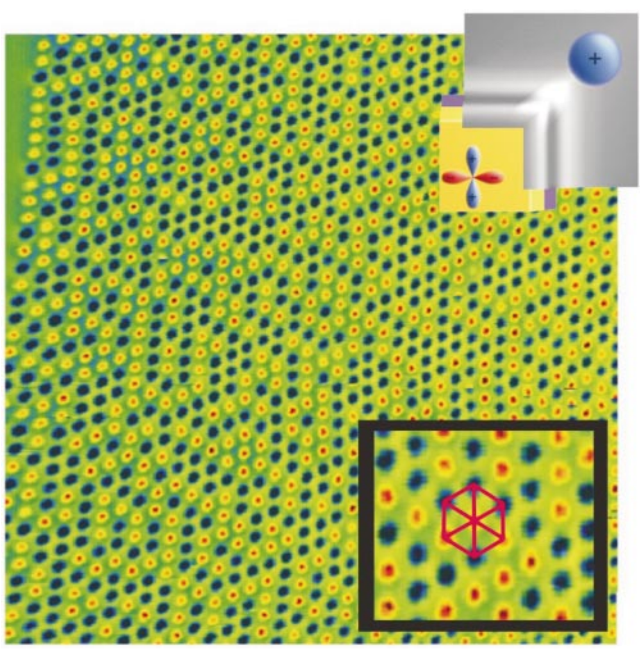

Figure 2 Scanning SQUID micrograph of the flux state in a section of a triangular lattice ($T = 4.2$ K). Each dot represents a half-fluxon, generated by a corner junction with a facet length of 5 μm, shown schematically at top right. All corner junctions are electrically isolated from each other, and the distance between their centre points is 12 μm. At bottom right a 4× magnified area is shown, with an overlay of lines forming a body-centred hexagon connecting seven of the half flux quanta, as an illustration of the triangular lattice geometry.

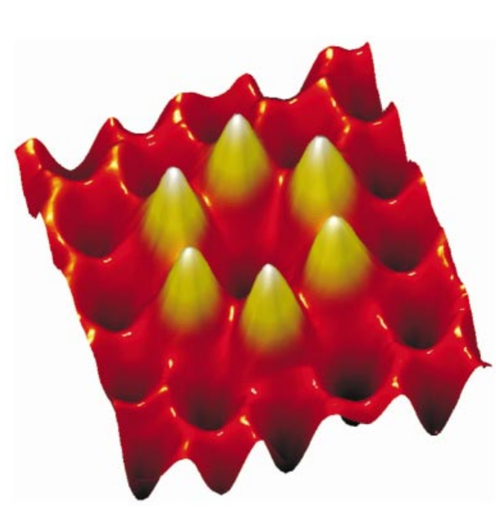

Figure 3 Scanning SQUID micrograph of a two-dimensional triangular array of π-loops (10-μm-wide facets, 25-μm spacing) in an 80 μm × 80 μm area. In this array, a hexagonal pattern of six half flux quanta was written by reversing the polarity of selected elements at zero field and $T = 4.2$ K, after cooling in a magnetic field so that all half-fluxons initially have the same polarity. In this image, the dark-red valleys represent magnetic flux with opposite polarity to the flux represented by the yellow peaks.

the triangular lattice depicted in Fig. 2, σ was found to be -0.1, providing evidence for the predominant antiferromagnetic nearest-neighbour coupling of the individual half-integer flux quanta in this system. For the next-nearest-neighbour interaction, at a distance of $\sim$21 μm, σ was close to 0. It is probable that the pattern of half flux quanta shown in Fig. 2 includes some frozen-in disorder, as with the used cool-down speed of about 10 mK s^{-1}, the large-scale array will not have sufficient time to relax to an overall energetic ground state. This source of disorder may be reduced by lowering the cool-down speed.

The spontaneous currents generated in the elements of the triangular array of Fig. 2 were remarkably uniform, as indicated by a full-width at half-maximum of the distribution in peak amplitudes, which was about 0.28 times the average peak height. We do not believe that this observed spread is a dominant source of disorder in the π-ring array cooling experiments, because it will cause fluctuations in the magnitude, as opposed to fluctuations in the sign, of the ring–ring coupling. A detailed comparison between the ordering in two-dimensional half-fluxon lattices generated in frustrated and unfrustrated geometries—the latter including, for example, square and honeycomb lattices—is under investigation.

Once cooled down to $T = 4.2$ K, the energy required to alter the polarity of a half flux quantum is considerably larger than the thermal energy ($E_b \approx I_c\Phi_0/\pi > 10^4$ K), which is reflected in the temporal stability of the flux pattern. But by applying locally a magnetic field, it is possible to manipulate the polarity of the individual half-integer flux quanta, enabling the possibilities of storing information or of constructing desired patterns of fractional flux. This is demonstrated in Fig. 3, showing six half-fluxons in a hexagonal arrangement, with opposite polarity to the surrounding half flux quanta in this triangular lattice, spaced at 25 μm. The polarity of the half flux quanta in this sample with facet length $a = 10$ μm was set by scanning a SQUID susceptometer[31] over the junctions at a rate of 0.05 mm s^{-1} while applying a 2-mA current through the excitation coil (this coil is 21 μm in diameter, and concentric and co-planar with the 8 μm square SQUID pick-up loop). This corresponds to a field of approximately 50 μT at the junction. Reversing the current direction reversed the resultant polarity of the half-vortex. The critical field required to flip the polarity of the half-vortex is in rough agreement with numerical calculations[32]. We expect that, apart from the spontaneous flux formation, the writing of half flux quanta patterns will provide a diverse basis for both fundamental studies and potential applications. □

Received 14 October 2002; accepted 14 January 2003; doi:10.1038/nature01442.

1. Bardeen, J., Cooper, L. N. & Schrieffer, J. R. Theory of superconductivity. *Phys. Rev.* **108,** 1175–1204 (1957).
2. Deaver, B. S. Jr & Fairbank, W. M. Experimental evidence for quantized flux in superconducting cylinders. *Phys. Rev. Lett.* **7,** 43–46 (1961).
3. Doll, R. & Näbauer, M. Experimental proof of magnetic flux quantization in a superconducting ring. *Phys. Rev. Lett.* **7,** 51–52 (1961).
4. Geshkenbein, V. B. & Larkin, A. I. The Josephson effect in superconductors with heavy fermions. *JETP Lett.* **43,** 395–399 (1986).
5. Geshkenbein, V. B., Larkin, A. I. & Barone, A. Vortices with half magnetic flux quanta in "heavy-fermion" superconductors. *Phys. Rev. B* **36,** 235–238 (1987).
6. Sigrist, M. & Rice, T. M. Paramagnetic effect in high-T_c superconductors—a hint for *d*-wave superconductivity. *J. Phys. Soc. Jpn* **61,** 4283–4286 (1992).
7. Tsuei, C. C. & Kirtley, J. R. Pairing symmetry in cuprate superconductors. *Rev. Mod. Phys.* **72,** 969–1016 (2000).
8. Bulaevskii, L. N., Kuzii, V. V. & Sobyanin, A. A. Superconducting system with weak coupling to the current in the ground state. *JETP Lett.* **25,** 290–294 (1977).
9. Van Harlingen, D. J. Phase-sensitive tests of the symmetry of the pairing state in the high-temperature superconductors—Evidence for d_{x2-y2} symmetry. *Rev. Mod. Phys.* **67,** 515–535 (1995).
10. Schulz, R. R. *et al.* Design and realization of an all *d*-wave dc π-superconducting quantum interference device. *Appl. Phys. Lett.* **76,** 912–914 (2000).
11. Smilde, H. J. H. *et al.* *d*-Wave-induced Josephson current counterflow in $YBa_2Cu_3O_7$/Nb zigzag junctions. *Phys. Rev. Lett.* **88,** 057004 (2002).
12. Smilde, H. J. H., Hilgenkamp, H., Rijnders, G., Rogalla, H. & Blank, D. H. A. Enhanced transparency ramp-type Josephson contacts through interlayer deposition. *Appl. Phys. Lett.* **80,** 4579–4581 (2002).
13. Aeppli, G. & Chandra, P. Seeking a simple complex system. *Science* **275,** 177–178 (1997).
14. Moessner, R. & Sondhi, S. L. Ising models of quantum frustration. *Phys. Rev. B* **63,** 224401 (2001).
15. Chandra, P. & Doucot, B. Possible spin-liquid state at large S for the frustrated square Heisenberg lattice. *Phys. Rev. B* **38,** 9335–9338 (1988).
16. Davidovic, D. *et al.* Magnetic correlations, geometrical frustration, and tunable disorder in arrays of superconducting rings. *Phys. Rev. B* **55,** 6518–6540 (1997).
17. Pannetier, B., Chaussy, J., Rammal, R. & Villegier, J. C. Experimental fine tuning of frustration: Two-dimensional superconducting networks in a magnetic field. *Phys. Rev. Lett.* **53,** 1845–1848 (1984).
18. Lerch, Ph., Leemann, Ch., Theron, R. & Martinoli, P. Dynamics of the phase transition in proximity-effect arrays of Josephson junctions at full frustration. *Phys. Rev. B* **41,** 11579–11582 (1990).
19. Mooij, J. E. *et al.* Josephson persistent-current qubit. *Science* **285,** 1036–1039 (1999).
20. Van der Wal, C. *et al.* Quantum superposition of macroscopic persistent-current states. *Science* **290,** 773–777 (2000).
21. Friedman, J. R., Patel, V., Chen, W., Tolpygo, S. K. & Lukens, J. E. Quantum superposition of distinct macroscopic states. *Nature* **406,** 43–46 (2000).
22. Ioffe, L. B., Geshkenbein, V. B., Feigel'man, M. V., Fauchère, A. L. & Blatter, G. Environmentally decoupled sds-wave Josephson junctions for quantum computing. *Nature* **398,** 679–681 (1999).
23. Blais, A. & Zagoskin, A. Operation of universal gates in a solid-state quantum computer based on clean Josephson junctions between *d*-wave superconductors. *Phys. Rev. A* **61,** 042308 (2000).
24. Preskill, J. Reliable quantum computers. *Proc. R. Soc. Lond. A* **454,** 385–410 (1998).
25. Bennett, C. H. & DiVincenzo, D. P. Quantum information and computation. *Nature* **404,** 247–255 (2000).
26. Rogers, F. P. *A Device for Experimental Observation of Flux Vortices Trapped in Superconducting Thin Films*. Thesis, MIT, Boston (1983).
27. Vu, L. N. & Van Harlingen, D. J. Design and implementation of a scanning SQUID microscope. *IEEE Trans. Appl. Supercond.* **3,** 1918–1921 (1993).
28. Black, R. C. Magnetic microscopy using a liquid nitrogen cooled $YBa_2Cu_3O_7$ superconducting quantum interference device. *Appl. Phys. Lett.* **62,** 2128–2130 (1993).
29. Kirtley, J. R. *et al.* High-resolution scanning SQUID microscope. *Appl. Phys. Lett.* **66,** 1138–1140 (1995).
30. Cowley, J. M. An approximate theory of order in alloys. *Phys. Rev.* **77,** 669–675 (1950).
31. Gardner, B. W. *et al.* Scanning superconducting quantum interference device susceptometry. *Rev. Sci. Instrum.* **72,** 2361–2364 (2001).
32. Kirtley, J. R., Moler, K. A. & Scalapino, D. J. Spontaneous flux and magnetic-interference patterns in 0-π Josephson junctions. *Phys. Rev. B* **56,** 886–891 (1997).

Acknowledgements We thank R. H. Koch, J. Mannhart, D. M. Newns and D. J. Scalapino for discussions. This work was supported by the Dutch Foundation for Research on Matter (FOM), the Netherlands Organization for Scientific Research (NWO), the Royal Dutch Academy of Arts and Sciences (KNAW) and the European Science Foundation (ESF) PiShift programme.

Competing interests statement The authors declare that they have no competing financial interests.

Correspondence and requests for materials should be addressed to H.H. (e-mail: H.Hilgenkamp@utwente.nl).

Superconductivity in two-dimensional CoO_2 layers

Kazunori Takada*‡, Hiroya Sakurai†, Eiji Takayama-Muromachi†, Fujio Izumi*, Ruben A. Dilanian* & Takayoshi Sasaki*‡

* *Advanced Materials Laboratory, National Institute for Materials Science, Tsukuba, Ibaraki 305-0044, Japan*
† *Superconducting Materials Center, National Institute for Materials Science, Tsukuba, Ibaraki 305-0044, Japan*
‡ *CREST, Japan Science and Technology Corporation*

Since the discovery of high-transition-temperature (high-T_c) superconductivity in layered copper oxides[1], many researchers have searched for similar behaviour in other layered metal oxides involving 3*d*-transition metals, such as cobalt and nickel. Such attempts have so far failed, with the result that the copper oxide layer is thought to be essential for superconductivity. Here we report that $Na_xCoO_2 \cdot yH_2O$ ($x \approx 0.35$, $y \approx 1.3$) is a superconductor with a T_c of about 5 K. This compound consists of two-dimensional CoO_2 layers separated by a thick insulating layer of Na^+ ions and H_2O molecules. There is a marked resemblance in superconducting properties between the present material and high-T_c copper oxides, suggesting that the two systems have similar underlying physics.

The $Na_xCoO_2 \cdot yH_2O$ sample was obtained through a chemical

